Epigenetic Regulation of Adipogenesis by PHF2 Histone Demethylase

Yosuke Okuno,[1] Fumiaki Ohtake,[1] Katsuhide Igarashi,[2] Jun Kanno,[2] Takahiro Matsumoto,[1] Ichiro Takada,[1] Shigeaki Kato,[3] and Yuuki Imai[1]

PHF2 is a JmjC family histone demethylase that removes the methyl group from H3K9me2 and works as a coactivator for several metabolism-related transcription factors. In this study, we examined the in vivo role of PHF2 in mice. We generated *Phf2* floxed mice, systemic *Phf2* null mice by crossing *Phf2* floxed mice with *CMV-Cre* transgenic mice, and tamoxifen-inducible *Phf2* knockout mice by crossing *Phf2* floxed mice with *Cre-ERT2* transgenic mice. Systemic *Phf2* null mice had partial neonatal death and growth retardation and exhibited less adipose tissue and reduced adipocyte numbers compared with control littermates. Tamoxifen-induced conditional knockout of PHF2 resulted in impaired adipogenesis in stromal vascular cells from the adipose tissue of tamoxifen-inducible *Phf2* knockout mice as well as of *Phf2* knocked-down 3T3-L1 cells. PHF2 interacts with CEBPA and demethylates H3K9me2 in the promoters of CEBPA-regulated adipogenic genes. These findings suggest that PHF2 histone demethylase potentiates adipogenesis through interaction with CEBPA in vivo. Taken together, PHF2 may be a novel therapeutic target in the treatment of obesity and the metabolic syndrome. *Diabetes* 62:1426–1434, 2013

The architecture of eukaryotic chromatin is dynamically modulated by posttranslational modifications of the histones, including acetylation, phosphorylation, ubiquitination, and methylation (1). Methylation states of histones are crucial for chromatin reorganization and regulation of gene transcription. For example, lysine (K) methylation at H3K9, H3K27, and H4K20 is associated with regions of transcriptionally silenced chromatin, whereas methylation at H3K4, H3K36, and H3K79 is associated with transcriptionally active regions. Such modifications are controlled by a balance between enzymes that catalyze the addition and removal of methyl groups. LSD1 and the Jumonji C (JmjC) domain–containing proteins have been shown to possess such histone demethylase activities (2–4).

Plant homeodomain finger 2 (PHF2) is a newly characterized JmjC domain–containing protein identified as an interactant of nuclear receptors. PHF2 forms a complex with the AT-rich interactive domain 5B (ARID5B) and works as a coactivator for farnesoid X receptor (FXR) or hepatocyte nuclear factor 4 α (HNF4A). It is enzymatically inactive by itself but becomes an active H3K9me2 demethylase through protein kinase A (PKA)-mediated phosphorylation (5).

Although an increasing number of histone demethylases have been identified and their molecular functions progressively unraveled, the physiological functions of these demethylases remain largely unknown. Recently, LSD1 was reported to be required for embryogenesis (6), whereas JHDM2A is required for spermatogenesis (7) and obesity resistance (8) in vivo. In zebra fish, PHF8 and KDM7, which belong to the same subfamily of JmjC domain proteins as PHF2, regulate brain development (9,10). It has been suggested that PHF2 plays a role in induction of gluconeogenic genes by PKA signaling in hepatocytes (5) or rRNA expression in nucleoli (11) in vitro. However, in vivo analyses are required to explore the physiological role of PHF2. In this study, we generated PHF2 knockout mice and found that PHF2 plays a role in both neonatal growth and adipogenesis. These results imply that PHF2 demethylase function would be a novel translational target for human metabolic diseases.

RESEARCH DESIGN AND METHODS

Generation of *Phf2* floxed mice by gene targeting. A bacterial artificial chromosome (BAC) DNA containing mouse *Phf2* (BAC clone RP23-114C14) was obtained from the BAC-PAC Resources Center. *LoxP* was inserted between exons 6 and 7 of *Phf2* using the *Escherichia coli*-based BAC modification system (12). Modification cassettes were generated by PCR amplification of the PL452 vector with the following primers:5′-TATATAAGGAGCACTTGGGACCAGT-GACATACATGTGTCTAATGTCCTGAGAATTCATTCCGATCATATTCAATAACCC-3′ and 5′-ACTCTGGACACTAGGTGACCCAGTGGCCTCTCCTAATAGTTAATGAGCTC GAACTAGTGGATCCCCTCGA-3′. *LoxP*-inserted fragments of mouse *Phf2* were subcloned into the pBSIIKS+ vector using the *E. coli*-based BAC recombination system. Modification cassettes and retrieval cassettes were generated by PCR amplification of the pBSIIKS+ vector with primers corresponding to each promoter. *LacZ-PGK-Neo* was digested from the pNTR-lacZ-PGK-neo-lox vector and inserted into the pMC1DTpA vector that contained *DT-A*. Oligonucleotides of *loxP* and *frt* were inserted into this vector (cassette vector). *LoxP*-inserted fragments of mouse *Phf2* were inserted into the cassette vector to form the final *Phf2* knockout construct. The *Phf2* knockout construct was linearized by SacII and was introduced into M1 mouse embryonic cells (RIKEN) by electroporation and screened by genomic Southern blotting. Chimeric mice were generated by aggregation of embryonic stem cells with eight cell embryos of BDF1 mice. *Phf2^{Z/+}* mice were generated by crossing *Phf2^{N/+}* mice with *CMV-Cre* mice (13). *Phf2^{fl/+}* mice were generated by crossing *Phf2^{N/+}* mice with Flpe deleter strain ACTB-Flpe mice (Jackson Laboratory). Mice with *Phf2^{N/+}*, *Phf2^{Z/+}*, and *Phf2^{fl/+}* were maintained by backcrossing to C57BL/6J mice under a specific pathogen-free environment. All animals were maintained according to the protocol approved by the Animal Care and Use Committee of The University of Tokyo.

Generation of *Phf2* conditional knockout mice and genotyping. *Cre-ERT2* transgenic mice were provided by Dr. Daniel Metzger (14). *Cre-ERT2* transgenic mice were crossed with *Phf2^{fl/+}* mice to generate *Phf2^{fl/fl};Cre-ERT2* mice. Genotyping was performed by PCR using corresponding primers. Sequences of primers were as follows: P1, 5′-CACCCTCTGTGTCCTCCTGT-3′; P2, 5′-CAGTTCTCTTAGCTCCCCCTTT-3′; P3, 5′-GACAGGAAGCCAAGGA-GATG-3′; P4, 5′-GACAGCCTGGTCAGGTGAAT-3′; and P5, 5′-TGTAATACA-CCTGGGGCTCA-3′. *Cre-ERT2* transgenic mice were identified by amplification of the *Cre* allele using primers 5′-TTACGGCGCTAAGGATGACT-3′ and 5′-TTGCCCCTGTTTCACTATCC-3′.

Adipose tissue collection. Mice were killed by cervical dislocation. Epididymal, gonadal, lumbar subcutaneous, and mesenteric white adipose tissues (WATs) were carefully separated from testis, uterus, skin, and intestines, respectively. Wet weights of these WATs were measured.

Glucose and insulin tolerance tests. Food was removed 2 h before glucose (2 g/kg) or insulin (1 units/kg) was administered by intraperitoneal injection. Blood samples were collected from the tail vein at various times after the glucose load, as indicated. Plasma glucose was immediately determined on an Accu-Chek Aviva (Roche).

Cell culture. 3T3-L1 mouse fibroblasts were maintained and differentiated into adipocytes as previously described (15). Mouse primary embryonic fibroblasts were isolated on embryonic day 13.5 and cultured in Dulbecco's modified Eagle's medium with 10% FBS.

Plasmids. FLAG-tagged, full-length cDNAs of human CEBPA or PPARG were inserted into pcDNA3 vectors (Invitrogen).

Western blot. Protein levels were determined by blotting with anti-FLAG antibody (Sigma-Aldrich), anti-CEBPA antibody (Santa Cruz Biotechnology), and anti-PHF2 antibody (5). ECL Plus (Amersham) was used for detection of the immunoreactive bands.

mRNA analysis. Total RNA was isolated with TRIzol reagent (Invitrogen) according to the manufacturer's protocol. First-strand cDNA was synthesized from total RNA using PrimeScript RT Master Mix (Takara) and subjected to real-time PCR using KAPA SYBR Fast qPCR Kits (Kapa Biosystems) with Thermal Cycler Dice (Takara) according to the manufacturers' instructions. The following primers were used: mouse *Phf2*, 5′-TACTGCCTGATCTGTGT-GAAGGA-3′ and 5′-CTGGCCGGATGAGATAGAAGA-3′; mouse *Pparg*, 5′-TTA-ACTGCCGGATCCACAAAA-3′ and 5′-TGAGACATCCCCACAGCAAG-3′; mouse *Cebpa*, 5′-TGCCAAACTGAGACTCTTCACTAAC-3′ and 5′-CCCAAACATCCC-TAAACCAAAA-3′; mouse *Adipoq*, 5′-CAAGGCCGTTCTCTTCACCTAC-3′ and 5′-TCCCCATCCCCATACACCT-3′; mouse *Fabp4*, 5′-CAGCGTAAAATGGGGATT-TGG-3′ and 5′-GCTCTTCACCTTCCTGTCGTCT-3′; mouse *Plin2*, 5′-GAGCTG-GAGATGGAAGCAAAA-3′ and 5′-GTGATAAGCCCGAGAGCAGAG-3′; mouse *Cd36*, 5′-AAGAACAGCAGCAAAATCAAGG-3′ and 5′-AGACAGTGAAGGCTC-AAAGATGG-3′; mouse *Lpl*, 5′-TGGGACTGAGGATGGCAAG-3′ and 5′-GGCA-GGGTGAAGGGAATGT-3′; and mouse *Arbp*, 5′-GCTCCAAGCAGATGCAGCA-3′ and 5′-CCGGATGTGAGGCAGCAG-3′.

Retroviral infection. Platinum-E cells were transfected with either pSuper-retro-puro-shLacZ or pSuper-retro-puro-shPHF2 (5′-GCCTGACTCAGTTTCCCAACT-3′) using Lipofectamine (Invitrogen). Forty-eight hours after transfection, the medium containing retroviruses was harvested, filtered, and transferred to 3T3-L1 cells. Infected cells were selected with 1 μg/mL puromycin.

Chromatin immunoprecipitation assays. Chromatin immunoprecipitation (ChIP) assays were carried out essentially as previously described (16). For immunoprecipitation, antibody against CEBPA (sc-61; Santa Cruz Biotechnology) or PHF2 (5) was used. The precipitated DNA fragments were amplified by real-time PCR. The following primers were used: mouse *Cebpa*-CEBPRE, 5′-TTGCGC-CACGATCTCTCTC-3′ and 5′-CTTAGAGCCCGCCTTCTCCT-3′; mouse *Pparg*-CEBPRE, 5′-CCACTGGTGTGTATTTTACTGCAA-3′ and 5′-GTTCTGTGAGGGGCGT-GAA-3′; mouse *Fabp4*-CEBPRE, 5′-CATTGCCAGGGAGAACCAA-3′ and 5′-CCATGT-GACTGTAGGAGTGACCAA-3′; and mouse negative control region, 5′-CAGACATG-TCAAATCAAGAAGACAG-3′ and 5′-ACTTTGGAGGAAGAGGCAGAAA-3′.

Microarray analysis. These procedures were conducted according to the Percellome method (17). Briefly, mRNA expression values were normalized to the cell numbers in each sample by adding external spike mRNAs to them in proportion to the genomic DNA concentration and using the spike RNA quantity data as a dose-response standard curve for each sample. Total RNAs were purified from epididymal adipose tissue using an RNeasy Mini kit (Qiagen). First-strand cDNAs were synthesized using SuperScript II reverse transcriptase (Invitrogen). After second-strand synthesis, the double-stranded cDNAs were purified using a GeneChip (Affymetrix) Sample Cleanup Module and labeled by in vitro transcription using a BioArray HighYield RNA Transcript Labeling Kit (Enzo Life Sciences). The labeled cRNA was then purified using a GeneChip Sample Cleanup Module. Purified cRNA were hybridized with GeneChip Mouse Genome 430 2.0 Array. Washing and staining were performed in a GeneChip Fluidics Station using the appropriate antibody amplification, washing, and staining protocols. The phycoerythrin-stained arrays were scanned as digital image files, which were analyzed with GeneChip Operating Software. The expression data were converted to copy numbers of mRNA per cell by the Percellome method and analyzed using Percellome software.

Morphometric analysis. Paraffin sections of epididymal WAT were processed for hematoxylin-eosin staining and observed by light microscopy. Adipocyte areas were measured using OsteoMeasure.

Evaluation of adipocyte number. The number of adipocytes in epididymal WAT was estimated as previously described (18). Briefly, adipose tissue was minced and fixed at 37°C for 96 h in 1.88% osmium tetroxide. After washing twice with PBS, it was replaced with 8 mol/L urea at room temperature for 48

h. Urea-free particles were washed through a 180-μm net (Millipore), trapped on a 10-μm net (Millipore), and suspended using 0.01% Triton X-100 in PBS. Particles were counted with a counting chamber.

Oil red O staining. Cells were stained with oil red O, and the quantification was performed as previously described (19). Briefly, cells were fixed with 10% formalin and stained in a working solution of oil red O. Isopropyl alcohol was added to the stained culture dishes, and the extracted dye was monitored spectrophotometrically at 510 nm.

Statistical analysis. Data were analyzed by two-tailed Student *t* test, Pearson χ^2 test, log-rank test, or two-way repeated-measures ANOVA. For all graphs, data are presented as mean ± SEM. Statistical significance was accepted at $P < 0.05$.

RESULTS

Generation of *Phf2* floxed mice. Figure 1*A* shows the strategy to generate the mutant *Phf2* mutant allele. Successful insertion of *LacZ-PGK-Neo^R* cassettes and *loxP* at sites flanking exon 6 of the *Phf2* allele was confirmed by Southern blotting (Fig. 1*B*). Cre-mediated recombination excised exon 6 and *PGK-Neo^R* from the mutant allele, resulting in the *LacZ* allele. P1, P2, and P3 primers were used to differentiate the wild-type and *LacZ* alleles (Fig. 1*C*). Flpe-mediated recombination excised *LacZ* and *PGK-Neo^R* from the mutant allele, resulting in a floxed allele. P4 and P5 primers were used to differentiate the wild-type and floxed alleles (Fig. 1*D*). Cre-mediated recombination excised exon 6 from the floxed allele, resulting in a null allele. Exon 6 corresponds to part of the JmjC domain of *Phf2*, and its deletion is expected to result in an alteration of the reading frame of the *Phf2* transcript. As expected, the PHF2 protein was not detected in mouse embryonic fibroblasts of *Phf2$^{Z/Z}$* (Fig. 1*E*).

***Phf2$^{Z/Z}$* mice were characterized by partial neonatal death and postnatal growth retardation.** *Phf2$^{Z/Z}$* mice were born according to expected Mendelian ratios (Fig. 2*A*). However, <30% of *Phf2$^{Z/Z}$* pups were alive when they reached 2 weeks of age (Fig. 2*B*). In fact, daily observation revealed that ~70% of *Phf2$^{Z/Z}$* mice died within 3 days of birth ($P = 3.0 \times 10^{-5}$ compared with wild type) (Fig. 2*C*). However, after 3 days of age, the remaining pups retained viability and lived for no less than 6 months (data not shown). *Phf2$^{Z/Z}$* mice had progressively reduced growth compared with littermate controls until 10 days after birth, although there was little difference in body weight among newborn mice of different genotypes (Fig. 2*D*). Two weeks after birth, *Phf2$^{Z/Z}$* mice grew in a manner similar to wild-type or heterozygous littermates, but with significant differences in body weight (Fig. 2*E*). The extent of these weight reductions was not significantly different between males and females (two-way repeated-measures ANOVA). These data suggest that PHF2 is dispensable for the survival of embryos but is necessary for survival and growth in the neonatal period.

Reduced adipose tissue in *Phf2$^{Z/Z}$*. Next, we surveyed the weight and appearance of each tissue present in male *Phf2$^{Z/Z}$* mice at 5 weeks of age. As mentioned previously, *Phf2$^{Z/Z}$* mice had decreased body weights at that time (Fig. 3*A*). *Phf2$^{Z/Z}$* mice exhibited significantly shortened body lengths (Fig. 3*A*). Various tissues of *Phf2$^{Z/Z}$*, including brown adipose tissue (BAT), appeared normal and weighed the same as in control littermates. However, WAT and brain showed a different trend. The brain weights were significantly increased compared with wild-type littermates, the potential significance of which will be discussed later (Fig. 3*A*). The weight of epididymal WAT was only 50% of that found in control littermates, even when normalized by body weight. Weight reduction was also
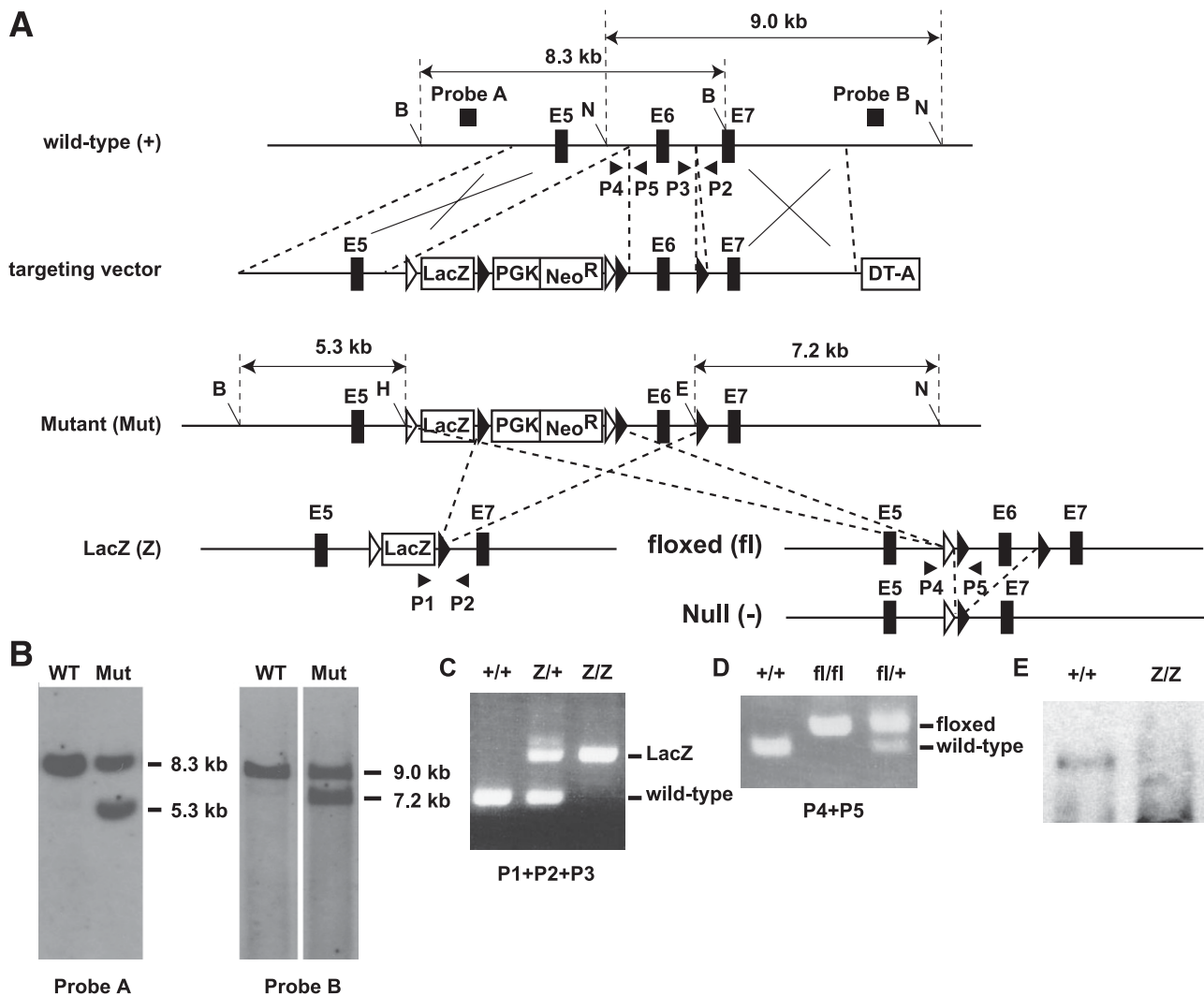
FIG. 1. Strategic scheme for targeted disruption of mouse *Phf2*. *A*: Targeting strategy with positive/negative selection. Strategy of genomic Southern blotting in the screening for homologous recombinant embryonic stem cell clones is also included. E5, E6, and E7 represent exon 5, exon 6, and exon 7 of *Phf2*, respectively. B, H, E, and N represent BglII, HindIII, EcoRI, and NsiI cut sites, respectively. P1, P2, P3, P4, and P5 represent locations of primers used in *C* and *D*. ▷, the *LoxP* sites; ▶, *Frt* sites. *B*: Southern blotting analysis of targeted embryonic stem cell clones. Restriction enzymes used for screening recombination events with probe A were BglII and HindIII. An 8.3-kb fragment in WT and a 5.3-kb fragment after homologous recombination were expected with probe A. Restriction enzymes used for screening recombination events with probe B were EcoRI and NsiI. A 9.0-kb fragment in WT and a 7.2-kb fragment after homologous recombination were expected with probe B. *C*: To detect the presence of the *LacZ* allele (Z) and the WT allele (+), primers P1, P2, and P3 were used. The PCR bands of the WT allele (242 bp) and the *LacZ* allele (495 bp) are indicated. *D*: To detect the presence of the floxed allele (fl) and the WT allele (+), primers P4 and P5 were used. The PCR bands of the WT allele (162 bp) and the floxed allele (245 bp) are indicated. *E*: Western blot analysis of PHF2 protein expression in *Phf2^{Z/Z}* mice. Extracts of mouse embryonic fibroblasts from WT or *Phf2^{Z/Z}* were immunoprecipitated and detected with anti-PHF2 antibody. WT, wild type.

observed in subcutaneous WAT to an extent similar to that in epididymal WAT ($P = 0.06$) but to a lesser extent in mesenteric WAT (Fig. 3*B*). Additionally, female *Phf2^{Z/Z}* mice exhibited a similar reduced weight of gonadal WAT as observed in male mice (Fig. 3*C*). However, these weight reductions in adipose tissues seemed to be limited to a young age because there was no significant difference of WAT weights between *Phf2^{Z/Z}* and wild-type littermates when the mice reached 8 weeks of age (Supplementary Fig. 1). To elucidate whether the decreased weight of WAT was caused by a reduction of lipid droplets per cell or adipocyte number, we measured adipocyte size and number in epididymal WAT of *Phf2^{Z/Z}* and wild-type littermates. Evaluation of the mean adipocyte area in the section of WAT revealed that *Phf2^{Z/Z}* mice have smaller adipocytes than do control littermates (Fig. 3*D*). Furthermore, counting the number of adipocytes in WAT revealed

that *Phf2^{Z/Z}* mice have fewer adipocytes in adipose tissue (Fig. 3*E*). These data suggest that the decreased weight of WAT in *Phf2^{Z/Z}* mice was caused by a reduction in both the size and the number of adipocytes. Because impaired adipogenesis often results in decreased size (20) and a decreased number of adipocytes, we used microarray analysis to compare the gene expression profiles in WAT between *Phf2^{Z/Z}* mice and control littermates. As a result, the expression of various genes associated with adipogenesis, such as *Pparg, Cebpa, Fabp4, Adipoq, LPL, Plin2,* and *Cd36*, tended to be decreased in *Phf2^{Z/Z}* mice (Supplementary Fig. 2). The expression levels of more than half of these genes were significantly reduced when confirmed by real-time quantitative PCR (qPCR) (Fig. 3*F*). These data suggest that decreased WAT weight in *Phf2^{Z/Z}* mice resulted, at least in part, from impaired adipogenesis in these mice. Finally, we measured insulin sensitivity in
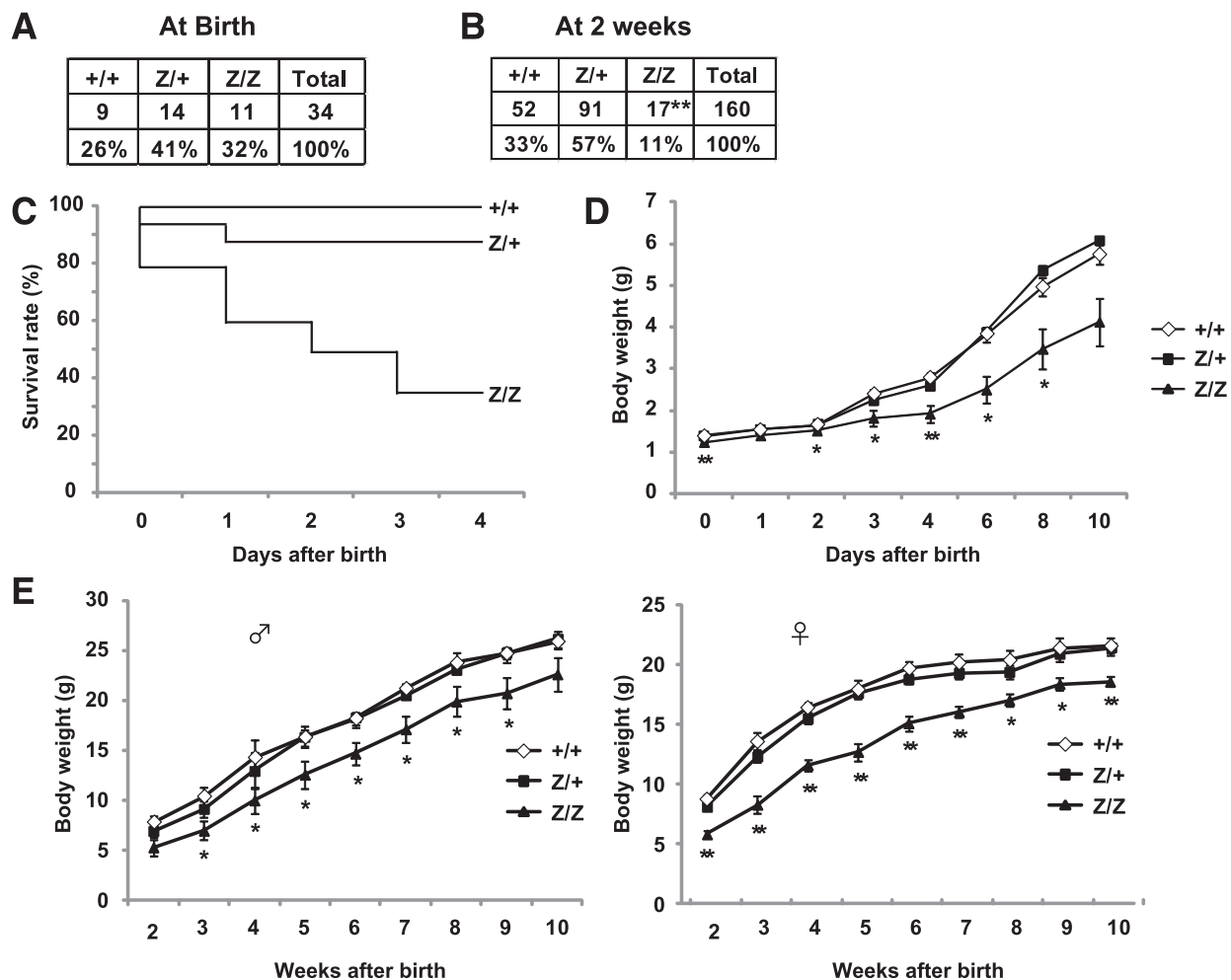
A **At Birth**

+/+	Z/+	Z/Z	Total
9	14	11	34
26%	41%	32%	100%

B **At 2 weeks**

+/+	Z/+	Z/Z	Total
52	91	17**	160
33%	57%	11%	100%

FIG. 2. Physiological features of systemic *Phf2* knockout mice. *A*: Genotypes of progeny of crosses between *Phf2*$^{Z/+}$ at birth. *B*: Genotypes of progeny of crosses between *Phf2*$^{Z/+}$ at 2 weeks of age. *C*: Survival rate of progeny of crosses between *Phf2*$^{Z/+}$. *D*: Growth curves of wild-type, heterozygous, and homozygous *Phf2* knockout mice until 10 days after birth. *E*: Growth curves of male mice and female mice of indicated genotypes between 2 and 10 weeks of age. ◇, wild-type mice (+/+); ■, heterozygous *Phf2* knockout mice (Z/+); ▲, homozygous *Phf2* knockout mice (Z/Z). *P < 0.05; **P < 0.01 compared with wild type.

Phf2$^{Z/Z}$ mice because adipose tissue is well known to be involved in glucose metabolism. There was no significant change in the glucose or insulin tolerance tests (Supplementary Fig. 3), suggesting that reduced WAT weight did not affect insulin sensitivity in mice at 5 weeks of age.

PHF2 is necessary for normal adipogenesis. To elucidate the role of PHF2 in adipogenesis, we generated *Phf2*$^{fl/fl}$; *Cre-ERT2* mice by crossing *Phf2* floxed mice with *Cre-ERT2* mice. Stromal vascular cells (SVCs) were then obtained from *Phf2*$^{fl/fl}$;*Cre-ERT2* mice or control *Cre-ERT2* mice and treated with 4-hydroxytamoxifen (4-OHT) to induce Cre-mediated excision of *Phf2*. As expected, treatment with 4-OHT efficiently reduced mRNA expression of *Phf2* in *Phf2*$^{fl/fl}$;*Cre-ERT2* but not in control *Cre-ERT2* mice (Fig. 4*C*). When SVCs were treated with a differentiation cocktail to induce their differentiation into adipocytes, differentiation was impaired in 4-OHT–treated SVCs from *Phf2*$^{fl/fl}$;*Cre-ERT2* mice as shown by oil red O staining (Fig. 4*A* and *B*). This was also confirmed by decreased expression of adipogenic marker genes in 4-OHT–treated SVCs from *Phf2*$^{fl/fl}$;*Cre-ERT2* mice (Fig. 4*C*). Next, we generated 3T3-L1 cell lines in which PHF2 was stably knocked down by retrovirus carrying *Phf2*-targeted short hairpin RNA. Infection of retrovirus carrying *shPhf2*

successfully decreased the expression of *Phf2* (Fig. 4*F*). In accordance with the results from SVCs, short hairpin RNA-mediated knockdown of *Phf2* resulted in impaired adipogenesis in the 3T3-L1 cell line as assessed by oil red O staining (Fig. 4*D* and *E*) and expression of adipogenic marker genes (Fig. 4*F*).

PHF2 is recruited with CEBPA to the promoter regions of adipogenic genes. The results indicated that PHF2 promoted adipogenesis. Moreover, we show that PHF2 works as a coactivator for several transcription factors through H3K9me2 demethylation (5). Therefore, we hypothesized that PHF2 coactivates transcription factors that promote adipogenesis. Among such transcription factors, PPARG and CEBPA are the master regulators for adipogenesis (21). First, we assessed whether PHF2 could physically interact with PPARG or CEBPA. When transfected into HEK293 cells, FLAG-CEBPA (but not FLAG-PPARG) was coimmunoprecipitated with endogenous PHF2 (Fig. 5*A*). Conversely, FLAG-PHF2 was coimmunoprecipitated with endogenous CEBPA in 3T3-L1 adipocytes (Fig. 5*B*). In accordance with these results, ChIP analysis revealed that PHF2 was recruited to known CEBPRE (CEBP responsive elements) in the promoter regions of *Cebpa*, *Pparg*, and *Fabp4* in differentiated
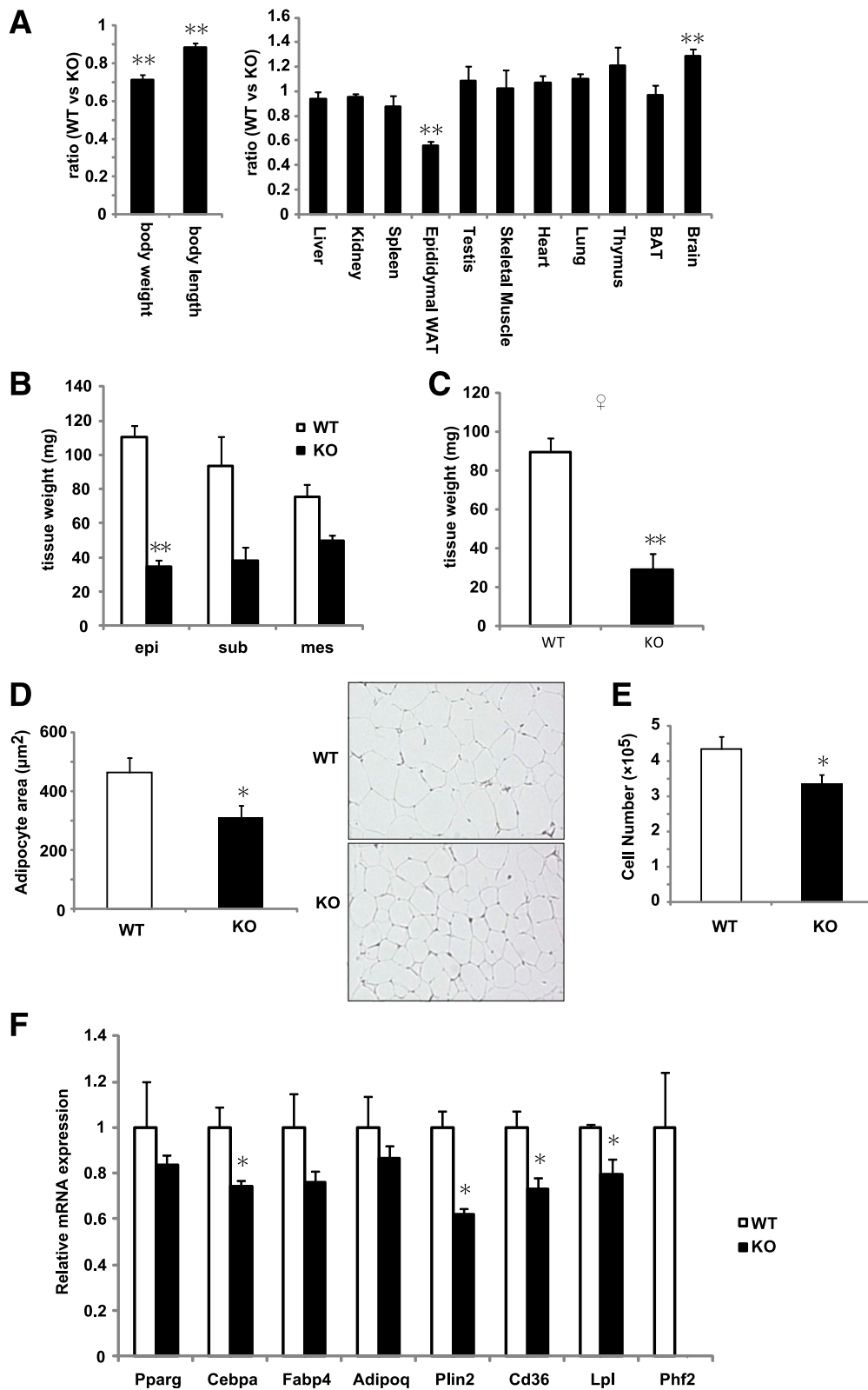
FIG. 3. Assessment of adipose tissue of systemic *Phf2* knockout mice. *A*: Ratio of body weight and nasoanal length or normalized tissue weight of male *Phf2^(Z/Z)* to WT littermates at 5 weeks of age. Tissue weights were normalized to body weights (*n* = 6). *B*: Weights of epididymal (epi) WAT, subcutaneous (sub) WAT, and mesenteric (mes) WAT of male *Phf2^(Z/Z)* KO mice and WT littermates at 5 weeks of age (*n* = 3). *C*: Weights of gonadal WAT of female *Phf2^(Z/Z)* KO mice and WT littermates at 5 weeks of age (*n* = 4). *D*: Mean adipocyte areas of epididymal WAT from *Phf2^(Z/Z)* KO mice and WT littermates (*n* = 5). High-magnification micrographs of WAT are shown. *E*: Adipocyte number in epididymal fat pads of *Phf2^(Z/Z)* KO mice and WT littermates (*n* = 7). *F*: Real-time qPCR analysis of adipocyte marker genes and *Phf2* of *Phf2^(Z/Z)* KO mice and WT littermates (*n* = 3). *P < 0.05; **P < 0.01 compared with WT. KO, knockout; WT, wild type. (A high-quality color representation of this figure is available in the online issue.)
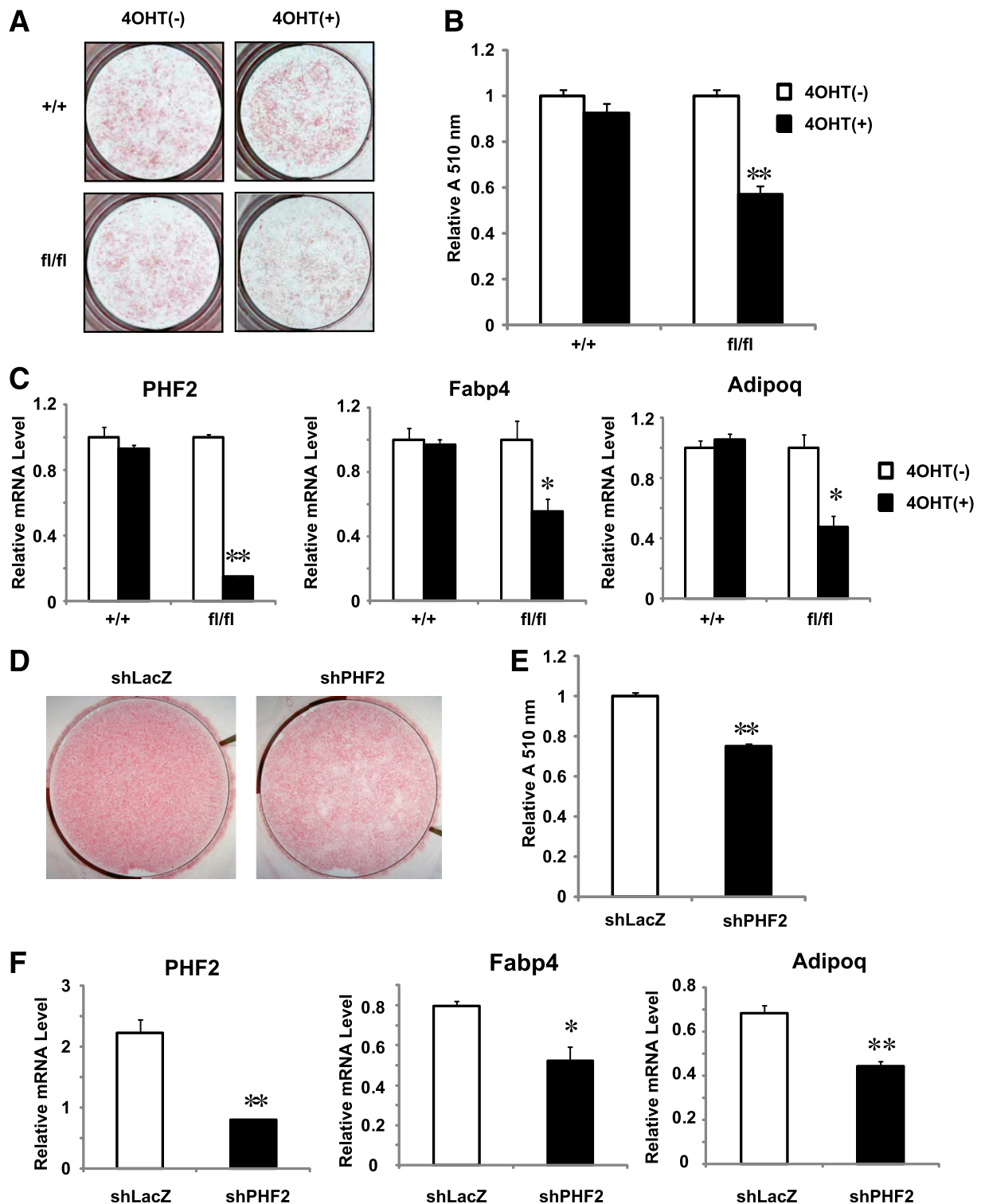
FIG. 4. Effects of PHF2 knock down on adipogenesis. *A–C*: SVCs from *Cre-ERT2; Phf2^fl/fl* (fl/fl) or *Cre-ERT2* (+/+) were treated with or without 4-OHT and differentiated into adipocytes by treatment with insulin, dexamethasone, and isobutylmethylxanthine. Image (*A*) and quantification (*B*) of oil red O staining and the results of real-time qPCR analysis of adipocyte marker genes (*C*) are shown (*n* = 3). *D–F*: 3T3-L1 cells infected with retroviruses containing either pSuper-retro-shLacZ or pSuper-retro-shPHF2 were differentiated into adipocytes. Image (*D*) and quantification (*E*) of oil red O staining and the results of real-time qPCR analysis of adipocyte marker genes (*F*) are shown (*n* = 3). *P < 0.05; **P < 0.01 compared with control.

3T3-L1 adipocytes (Fig. 5*C*). These results indicate that PHF2 might work as a coactivator for CEBPA. PHF2 seemed to be necessary for recruitment of CEBPA to chromatin because the recruitment of CEBPA to CEBPRE was impaired in 3T3-L1 in which *Phf2* had been knocked down (Fig. 5*D*). Moreover, modification of H3K9me2 in these CEBPRE was significantly increased in *Phf2* knocked-down 3T3-L1 adipocytes (Fig. 5*E*). These data indicate that PHF2 can play
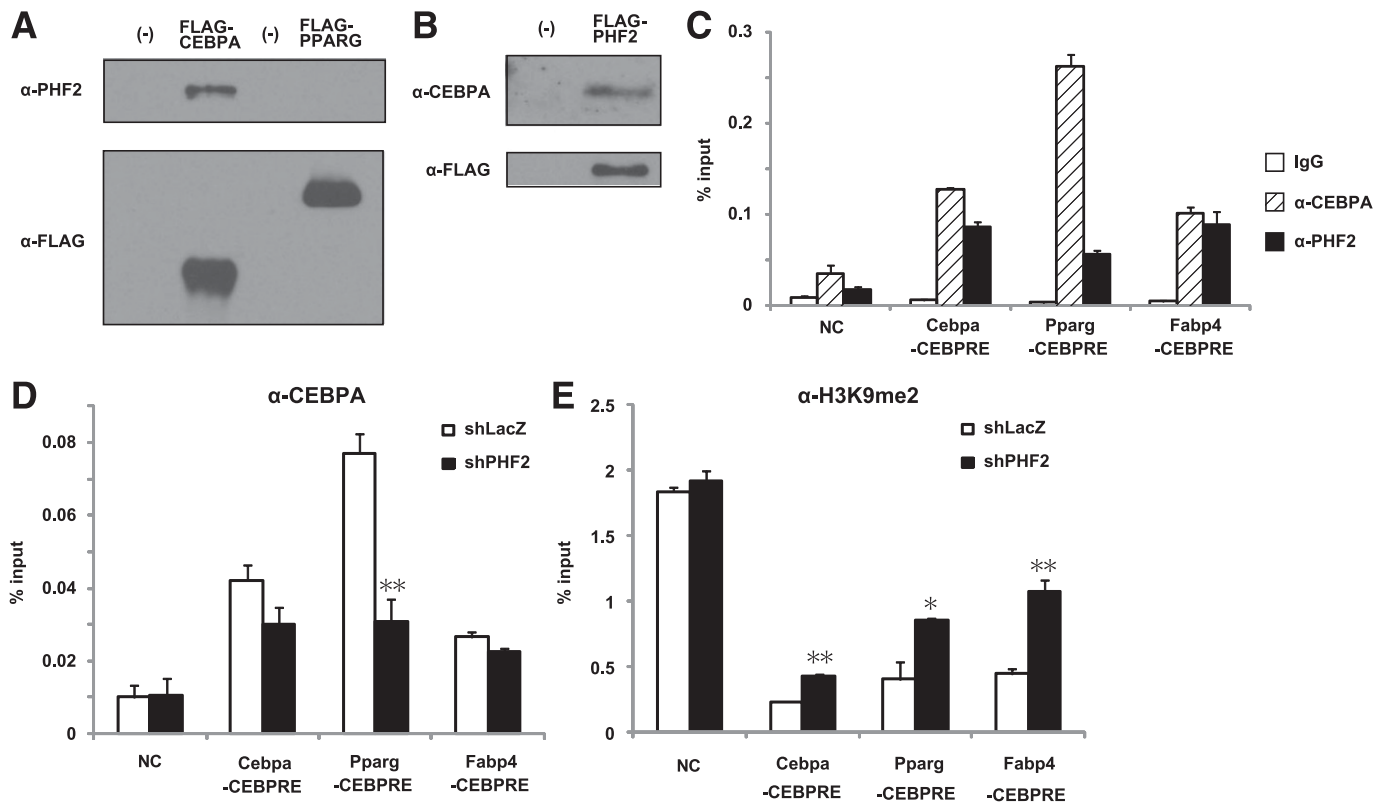
FIG. 5. Association of PHF2 with CEBPA. *A*: FLAG-CEBPA or FLAG-PPARG was transfected into HEK293T cells. Cells were harvested and immunoprecipitated with anti-FLAG antibody and detected with anti-PHF2 antibody or anti-FLAG antibody. *B*: FLAG-PHF2 was transfected into 3T3-L1 adipocytes. Cells were harvested and immunoprecipitated with anti-FLAG antibody and detected with anti-CEBPA antibody or anti-FLAG antibody. *C*: 3T3-L1 cells were fixed in formaldehyde on day 4 after differentiation, after which chromatin samples were subjected to ChIP analysis with indicated antibodies and amplified with primers toward indicated loci (*n* = 3). *D* and *E*: 3T3-L1 cells stably transfected with pSuper-retro-shLacZ or pSuper-retro-shPHF2 were differentiated into adipocytes and subjected to ChIP analysis with anti-CEBPA (*D*) or anti-H3K9me2 antibody (*E*), with primers toward the indicated loci (*n* = 3). *P < 0.05; **P < 0.01 compared with control. NC, negative control region.

a role as a coactivator, positively regulating adipogenic gene expression with CEBPA through H3K9me2 demethylation near CEBPA-binding regions.

DISCUSSION

To investigate the role of PHF2 in vivo, we generated *Phf2* knockout mice. *Phf2* knockout mice showed partial neonatal death, growth retardation, and reduced body weight. Reduced body weight seems to be mainly related to growth retardation and reduced lean mass in the knockout mice rather than reduced WAT mass because the body weight of *Phf2* knockout mice is still significantly lower than that of wild type at 8 weeks of age (Fig. 2*E*) when the weight of WAT is not different between *Phf2* knockout and wild type (Supplementary Fig. 1). The reason for this phenotype is not clear. PHF2 has been reported to be highly expressed in the neural tube and dorsal root ganglia (22), and *Phf2* represents a candidate gene for hereditary sensory neuropathy type I (HSN1) (23). In fact, the brain weights of *Phf2* knockout mice were larger than wild-type littermates. Taken together, we speculate that *Phf2* knockout mice may exhibit partial neonatal death attributable to defects in the central nervous system. Conditional deletion mutants using brain-specific Cre mice would clarify the precise roles of PHF2 in brain development.

On the other hand, subsequent study revealed that PHF2 plays an important role in adipogenesis. *Phf2* knockout mice produced lipoatrophy in which adipocytes were decreased in size and number. It seemed to be limited to a young age; for example, in *Klf5* knockout mice, atrophic changes in adipose tissue were abolished until 4 weeks of age (20). Although the reduced WAT phenotype in *Phf2* knockout mice disappeared after the mice reached 8 weeks of age and *Phf2* was systemically knocked out in these mice, this phenotype should be the result of a cell-autonomous mechanism because conditional knockout of *Phf2* in primary SVCs obtained from *Phf2^{fl/fl}*;*Cre-ERT* mice resulted in impaired adipogenesis. Moreover, PHF2 interacts with CEBPA, one of the master adipogenic regulators, and is recruited to CEBPRE. In addition, the lipoatrophic changes in *Phf2* knockout mice were stronger in epididymal and subcutaneous WAT than in mesenteric WAT, suggesting that PHF2 may be a possible candidate factor that determines regional variations in adipogenesis reported previously (24). Although adipose tissue is well known to be involved in glucose homeostasis, there was no significant change in glucose metabolism in *Phf2* knockout mice (Supplementary Fig. 3). There are two possible reasons for this result. First, 5 weeks of age is too young to develop insulin resistance, and second, only slight lipoatrophic change was observed in mesenteric WAT, the mass of which is strongly correlated with insulin resistance. It is meaningful to evaluate glucose metabolism of *Phf2* knockout adult mice under the treatment of a high-fat diet to clarify whether PHF2 plays a role in diabetes.

It is well known that factors that increase cAMP, such as isobutylmethylxanthine, strongly accelerate adipogenesis

(25). Elevation of cAMP is known to lead to suppression of Wnt10b (26) and Sp1 (27), induction of C/EBPβ (28), and production of PPARγ ligands (29). Moreover, cAMP signaling is mediated by two major pathways, PKA and Epac (exchange proteins directly activated by cAMP), that synergistically induce adipogenesis (30). However, it is not fully understood how PKA stimulates adipogenesis. PHF2 seems to be one possible candidate because it is reportedly activated through phosphorylation by PKA (5), and the current study shows that PHF2 stimulates adipogenesis. It seems that *Phf2* was not transcriptionally regulated during adipogenesis (Supplementary Fig. 4). However, PHF2 might be activated by PKA-mediated phosphorylation by a cAMP inducer in the adipogenic differentiation cocktail.

On the other hand, the weight reduction of BAT was not observed in *Phf2* knockout mice, although PKA and CEBPA were also reported to be necessary for the development of BAT (31). Recently, it was reported that brown adipocytes were differentiated from Myf5-positive precursor cells, which are more closely related to myoblasts rather than to the white preadipocytes (32). Thus, PHF2 may play a role in white preadipocytes but not in brown preadipocytes or myoblasts because the histone demethylases seem to be involved in differentiation in specific cell types.

PHF2 reportedly interacts with ARID5B, which is necessary for the coactivator function of PHF2 (5). Because phenotypes of systemic *Arid5b* knockout animals have already been reported (33–35), it is worth comparing the phenotypes between *Arid5b* knockout and *Phf2* knockout mice. Of note, most *Arid5b* knockout mice die within 24 h of birth, but some pups survive (33). The surviving *Arid5b* knockout animals show dramatically reduced body weight in neonates and adults. The WAT of *Arid5b* knockout mice weighed less than controls because of a reduction in the amount of lipid per cell. Because the phenotype of *Arid5b* knockout mice is close to that of *Phf2* knockout mice, it is likely that PHF2 and ARID5B work together in multiple organs, including adipose tissue.

Transcriptional control of the adipocyte lineage has been studied extensively (21,36). However, little is known about the role of histone demethylases during adipogenesis, even though several studies have clarified the roles of histone deacetylase HDAC1 (37,38) and HDAC3 (39) and histone demethylase LSD1 (40) in adipogenesis. In the current study, we found that histone demethylase PHF2 plays an important role in adipogenesis in vivo. Notably, several studies reported the role of histone demethylation in cell differentiation; for example, LSD1 controls pituitary terminal cell-type differentiation (6), JMJD3, an H3K27me3 demethylase, potentiates epidermal differentiation (41); and JMJD1A, an H3K9 demethylase, potentiates smooth muscle cell differentiation (42). In general, histone demethylases may play roles in cell differentiation in specific cell types. We suggest that PHF2 may be a significant histone demethylase in adipocytogenesis.

Adipose tissue plays an essential role in energy homeostasis. In mammals, WAT stores excess energy as triglycerides from fatty acids imported from circulating lipoproteins. Moreover, recent studies established adipose tissue as an active endocrine organ that secretes various humoral factors called adipokines that work in various physiological pathways, such as feeding, insulin resistance, inflammation, and atherogenesis (43). Thus, clarifications of precise molecular mechanisms that control adipose tissue development should improve our understanding of the

pathogenesis and pathophysiology of the metabolic syndrome, diabetes, and other metabolism-related diseases. In this study, PHF2 appears to be a novel molecule that controls adipogenesis in vivo. Modulation of enzymatic activities has been a good target of small molecules. In fact, some drugs that can modulate the activities of histone-modifying enzymes have been developed for clinical use (44–46). Thus, pharmacological modulation of the histone demethylase activity of PHF2 may be a new target in the treatment of human lipodystrophies or adipocyte hyperplasia in diet-induced obesity.

REFERENCES

1. Jenuwein T, Allis CD. Translating the histone code. Science 2001;293:1074–1080
2. Klose RJ, Kallin EM, Zhang Y. JmjC-domain-containing proteins and histone demethylation. Nat Rev Genet 2006;7:715–727
3. Shi Y. Histone lysine demethylases: emerging roles in development, physiology and disease. Nat Rev Genet 2007;8:829–833
4. Agger K, Christensen J, Cloos PA, Helin K. The emerging functions of histone demethylases. Curr Opin Genet Dev 2008;18:159–168
5. Baba A, Ohtake F, Okuno Y, et al. PKA-dependent regulation of the histone lysine demethylase complex PHF2-ARID5B. Nat Cell Biol 2011;13:668–675
6. Wang J, Scully K, Zhu X, et al. Opposing LSD1 complexes function in developmental gene activation and repression programmes. Nature 2007;446:882–887
7. Okada Y, Scott G, Ray MK, Mishina Y, Zhang Y. Histone demethylase JHDM2A is critical for *Tnp1* and *Prm1* transcription and spermatogenesis. Nature 2007;450:119–123
8. Tateishi K, Okada Y, Kallin EM, Zhang Y. Role of Jhdm2a in regulating metabolic gene expression and obesity resistance. Nature 2009;458:757–761
9. Qi HH, Sarkissian M, Hu GQ, et al. Histone H4K20/H3K9 demethylase PHF8 regulates zebrafish brain and craniofacial development. Nature 2010;466:503–507
10. Tsukada Y, Ishitani T, Nakayama KI. KDM7 is a dual demethylase for histone H3 Lys 9 and Lys 27 and functions in brain development. Genes Dev 2010;24:432–437
11. Wen H, Li J, Song T, et al. Recognition of histone H3K4 trimethylation by the plant homeodomain of PHF2 modulates histone demethylation. J Biol Chem 2010;285:9322–9326
12. Lee EC, Yu D, Martinez de Velasco J, et al. A highly efficient *Escherichia coli*-based chromosome engineering system adapted for recombinogenic targeting and subcloning of BAC DNA. Genomics 2001;73:56–65

13. Dupé V, Davenne M, Brocard J, et al. In vivo functional analysis of the Hoxa-1 3′ retinoic acid response element (3′RARE). Development 1997; 124:399–410

14. Ruzankina Y, Pinzon-Guzman C, Asare A, et al. Deletion of the developmentally essential gene *ATR* in adult mice leads to age-related phenotypes and stem cell loss. Cell Stem Cell 2007;1:113–126

15. Iwaki M, Matsuda M, Maeda N, et al. Induction of adiponectin, a fat-derived antidiabetic and antiatherogenic factor, by nuclear receptors. Diabetes 2003;52:1655–1663

16. Ohtake F, Baba A, Takada I, et al. Dioxin receptor is a ligand-dependent E3 ubiquitin ligase. Nature 2007;446:562–566

17. Kanno J, Aisaki K, Igarashi K, et al. "Per cell" normalization method for mRNA measurement by quantitative PCR and microarrays. BMC Genomics 2006;7:64

18. Mersmann HJ, MacNeil MD. Variables in estimation of adipocyte size and number with a particle counter. J Anim Sci 1986;62:980–991

19. Ramírez-Zacarías JL, Castro-Muñozledo F, Kuri-Harcuch W. Quantitation of adipose conversion and triglycerides by staining intracytoplasmic lipids with Oil red O. Histochemistry 1992;97:493–497

20. Oishi Y, Manabe I, Tobe K, et al. Krüppel-like transcription factor KLF5 is a key regulator of adipocyte differentiation. Cell Metab 2005;1:27–39

21. Farmer SR. Transcriptional control of adipocyte formation. Cell Metab 2006;4:263–273

22. Hasenpusch-Theil K, Chadwick BP, Theil T, Heath SK, Wilkinson DG, Frischauf AM. PHF2, a novel PHD finger gene located on human chromosome 9q22. Mamm Genome 1999;10:294–298

23. Nicholson GA, Dawkins JL, Blair IP, et al. The gene for hereditary sensory neuropathy type I (HSN-I) maps to chromosome 9q22.1-q22.3. Nat Genet 1996;13:101–104

24. Tchkonia T, Giorgadze N, Pirtskhalava T, et al. Fat depot origin affects adipogenesis in primary cultured and cloned human preadipocytes. Am J Physiol Regul Integr Comp Physiol 2002;282:R1286–R1296

25. Yarwood SJ, Anderson NG, Kilgour E. Cyclic AMP modulates adipogenesis in 3T3-F442A cells. Biochem Soc Trans 1995;23:175S

26. Bennett CN, Ross SE, Longo KA, et al. Regulation of Wnt signaling during adipogenesis. J Biol Chem 2002;277:30998–31004

27. Tang QQ, Jiang MS, Lane MD. Repressive effect of Sp1 on the C/EBPalpha gene promoter: role in adipocyte differentiation. Mol Cell Biol 1999;19: 4855–4865

28. Yeh WC, Cao Z, Classon M, McKnight SL. Cascade regulation of terminal adipocyte differentiation by three members of the C/EBP family of leucine zipper proteins. Genes Dev 1995;9:168–181

29. Tzameli I, Fang H, Ollero M, et al. Regulated production of a peroxisome proliferator-activated receptor-gamma ligand during an early phase of adipocyte differentiation in 3T3-L1 adipocytes. J Biol Chem 2004;279: 36093–36102

30. Petersen RK, Madsen L, Pedersen LM, et al. Cyclic AMP (cAMP)-mediated stimulation of adipocyte differentiation requires the synergistic action of Epac- and cAMP-dependent protein kinase-dependent processes. Mol Cell Biol 2008;28:3804–3816

31. Wang ND, Finegold MJ, Bradley A, et al. Impaired energy homeostasis in C/EBP alpha knockout mice. Science 1995;269:1108–1112

32. Seale P, Bjork B, Yang W, et al. PRDM16 controls a brown fat/skeletal muscle switch. Nature 2008;454:961–967

33. Whitson RH, Tsark W, Huang TH, Itakura K. Neonatal mortality and leanness in mice lacking the ARID transcription factor Mrf-2. Biochem Biophys Res Commun 2003;312:997–1004

34. Lahoud MH, Ristevski S, Venter DJ, et al. Gene targeting of Desrt, a novel ARID class DNA-binding protein, causes growth retardation and abnormal development of reproductive organs. Genome Res 2001;11:1327–1334

35. Schmahl J, Raymond CS, Soriano P. PDGF signaling specificity is mediated through multiple immediate early genes. Nat Genet 2007;39:52–60

36. MacDougald OA, Lane MD. Transcriptional regulation of gene expression during adipocyte differentiation. Annu Rev Biochem 1995;64:345–373

37. Wiper-Bergeron N, Wu D, Pope L, Schild-Poulter C, Haché RJ. Stimulation of preadipocyte differentiation by steroid through targeting of an HDAC1 complex. EMBO J 2003;22:2135–2145

38. Yoo EJ, Chung JJ, Choe SS, Kim KH, Kim JB. Down-regulation of histone deacetylases stimulates adipocyte differentiation. J Biol Chem 2006;281: 6608–6615

39. Fajas L, Egler V, Reiter R, et al. The retinoblastoma-histone deacetylase 3 complex inhibits PPARgamma and adipocyte differentiation. Dev Cell 2002;3:903–910

40. Musri MM, Carmona MC, Hanzu FA, Kaliman P, Gomis R, Párrizas M. Histone demethylase LSD1 regulates adipogenesis. J Biol Chem 2010;285: 30034–30041

41. Sen GL, Webster DE, Barragan DI, Chang HY, Khavari PA. Control of differentiation in a self-renewing mammalian tissue by the histone demethylase JMJD3. Genes Dev 2008;22:1865–1870

42. Lockman K, Taylor JM, Mack CP. The histone demethylase, Jmjd1a, interacts with the myocardin factors to regulate SMC differentiation marker gene expression. Circ Res 2007;101:e115–e123

43. Flier JS. Obesity wars: molecular progress confronts an expanding epidemic. Cell 2004;116:337–350

44. McCabe MT, Ott HM, Ganji G, et al. EZH2 inhibition as a therapeutic strategy for lymphoma with EZH2-activating mutations [letter to the editor online], 2012. Available from http://www.nature.com/nature/journal/vaop/ncurrent/full/nature11606.html. Accessed 2 November 2012

45. Song SH, Han SW, Bang YJ. Epigenetic-based therapies in cancer: progress to date. Drugs 2011;71:2391–2403

46. Tan J, Cang S, Ma Y, Petrillo RL, Liu D. Novel histone deacetylase inhibitors in clinical trials as anti-cancer agents. J Hematol Oncol 2010;3:5